Effects of film growth kinetics on grain coarsening and grain shape

F. D. A. Aarão Reis[*]

Instituto de Física, Universidade Federal Fluminense, Avenida Litorânea s/n, 24210-340 Niterói RJ, Brazil

We study models of grain nucleation and coarsening during the deposition of a thin film using numerical simulations and scaling approaches. The incorporation of new particles in the film is determined by lattice growth models in three different universality classes, with no effect of the grain structure. The first model of grain coarsening is similar to that proposed by Saito and Omura [Phys. Rev. E **84**, 021601 (2011)], in which nucleation occurs only at the substrate, and the grain boundary evolution at the film surface is determined by a probabilistic competition of neighboring grains. The surface grain density has a power-law decay, with an exponent related to the dynamical exponent of the underlying growth kinetics, and the average radius of gyration scales with the film thickness with the same exponent. This model is extended by allowing nucleation of new grains during the deposition, with constant but small rates. The surface grain density crosses over from the initial power law decay to a saturation; at the crossover, the time, grain mass, and surface grain density are estimated as a function of the nucleation rate. The distributions of grain mass, height, and radius of gyration show remarkable power law decays, similar to other systems with coarsening and particle injection, with exponents also related to the dynamical exponent. The scaling of the radius of gyration with the height h relative to the base of the grain show clearly different exponents in growth dominated by surface tension and growth dominated by surface diffusion; thus it may be interesting for investigating the effects of kinetic roughening on grain morphology. In growth dominated by surface diffusion, the increase of grain size with temperature is observed.

I. INTRODUCTION

The polycrystalline structure of a thin film controls its physical properties and consequently determines the possible technological applications [1]. This motivated the development of several models in the last three decades. Some of them are stochastic models on lattices, which may provide a realistic description of atomistic processes with much less computational effort than molecular dynamics and other *ab initio* methods. Reference [2] proposed one of the first models of this type: a finite number of labels was assigned to the atoms in a flat film surface, with a grain boundary dynamics that resembling the Potts model. Reference [3] adopted the same representation of crystalline grains in a kinetic Monte Carlo algorithm which was an extension of the Clarke-Vvedensky (CV) model for thin film deposition [4,5]. Subsequent works considered CV-type models but labeled the crystalline grain by a continuously varying angle that represents the orientation as it nucleates at the substrate [6–11]. These models couple the film growth with the grain boundary evolution. Recent approaches consider similar rules for labeling grains but simplify the bulk dynamics in comparison with the outer surface dynamics [12–16]. This allows the simulation of thick films (10^4 monolayers or more) and improves the model by accounting for the presence of defects and voids. There are also several models of grain boundary evolution that do not describe the growth dynamics of the films or bulk samples [17–20]. The study of grain boundaries in thermal equilibrium predicts relevant physical and chemical properties and may also give information for the nonequilibrium growth dynamics, such as diffusion coefficients [18].

An important step of the recent work by Saito and Omura [15] was to relate the decay of the density of surface grains to the scaling of height fluctuations of the film surface in the ballistic deposition model [21,22]. That relation was recently extended to other ballistic-type models in two-dimensional substrates [16]. The density decay depends on the basic symmetries of the growth kinetics but does not depend on microscopic details of the aggregation mechanism. In that case, the growth was described by the Kardar-Parisi-Zhang (KPZ) equation [23]. An earlier study of TiN films showed that grain sizes followed the substrate patterns and might be much larger than (and independent of) intragrain column sizes and void sizes [24]. Thus, those observations also suggest that the mechanisms of grain coarsening are independent of such short wavelength surface features.

In this work, we advance along these lines by modeling the formation and coarsening of crystalline grains during thin film deposition and studying the relations with kinetic roughening. We consider different growth mechanisms, which include cases dominated by surface tension [Edwards-Wilkinson (EW) [25] and KPZ] and cases dominated by adatom surface diffusion [Villain-Lai-Das Sarma growth [26,27]]. The latter allows the investigation of temperature effects. The grain boundaries evolve at the film surface according to a competition for capturing mobile atoms. We adopt the Saito-Omura approximation that neglects the effect of grain structure on the adatom surface mobility, with the advantage of allowing a clear demonstration of the effect of kinetic roughening on grain density scaling and grain shape.

Our first step is to extend the Saito-Omura work by considering nucleation of grains only at the substrate [15]. A scaling approach for predicting the decay of the grain density is generalized and confirmed by numerical simulations. Subsequently, we introduce a model in which new grains can be nucleated during the growth. The scaling of average grain

———————
[*]reis@if.uff.br

size, the size distribution, and other morphological features are explained along the same lines of other stochastic models with coarsening and particle injection [28,29]. The power-law decays of grain size distributions and the scaling of the grain shape (relation between average radius and height) are shown to depend on the dynamical exponent of the underlying kinetic roughening process. In all cases of diffusive surface dynamics, temperature increase favors formation of larger grains, in agreement with experimental observations.

The rest of this paper is organized as follows. In Sec. II we briefly review the models of film deposition and the universality classes of kinetic roughening. In Sec. III we present the model of grain coarsening with nucleation only at the substrate and study the properties of the polycrystalline samples for different processes of film deposition. In Sec. IV we present the model in which grain nucleation is possible at any film height and study the properties of samples produced with the same deposition processes. In Sec. VI we summarize our results and present our conclusions.

II. MODELS OF FILM DEPOSITION

The models are defined in a simple cubic lattice with a two-dimensional flat substrate of lateral size L at $z = 0$. The edge of a lattice site is taken as the unit length. Each deposited particle occupies one site at $z > 0$ and represents one atom or molecule, depending on the application. The term "column" is used to denote the set of particles of the deposit with position (x,y).

In all deposition models, the column of incidence of each particle is randomly chosen, the particle is released above the deposit and moves vertically towards the substrate ($-z$ direction), and the position of aggregation is chosen according to a set of stochastic or deterministic rules (in one of the models, the rules allow rejection of the aggregation attempt). A new particle is released only after the previous one is at its final position; these are called limited mobility (LM) models. The unit time is defined as the time necessary for aggregation (or attempt of aggregation) of L^2 particles, i.e., one monolayer.

The first deposition model is that of Family [30], which is also called random deposition with surface relaxation [22]. The incident particle aggregates at the column of incidence if no nearest neighbor (NN) column has smaller height. If only one NN has a smaller height, the particle moves to that column and aggregates there. If two or more NN columns have smaller heights, one of them is randomly chosen for the aggregation. These rules are illustrated in Fig. 1(a).

The second deposition model is the restricted solid-on-solid (RSOS) model [31]. The particle aggregates at the column of incidence if the differences of heights between nearest neighbor (NN) columns do not exceed 1. Otherwise, the aggregation attempt is rejected (i.e., rejection occurs only if the column of incidence is higher than some NN before the attempt). These rules are illustrated in Fig. 1(b).

The third deposition model is called lateral aggregation of diffusing particles (LADP). The incident particle reaches the film surface at the column of incidence and aggregates there if it has a lateral neighbor. Otherwise, it executes random steps to the top of NN columns and permanently aggregates when it encounters a lateral neighbor (during the
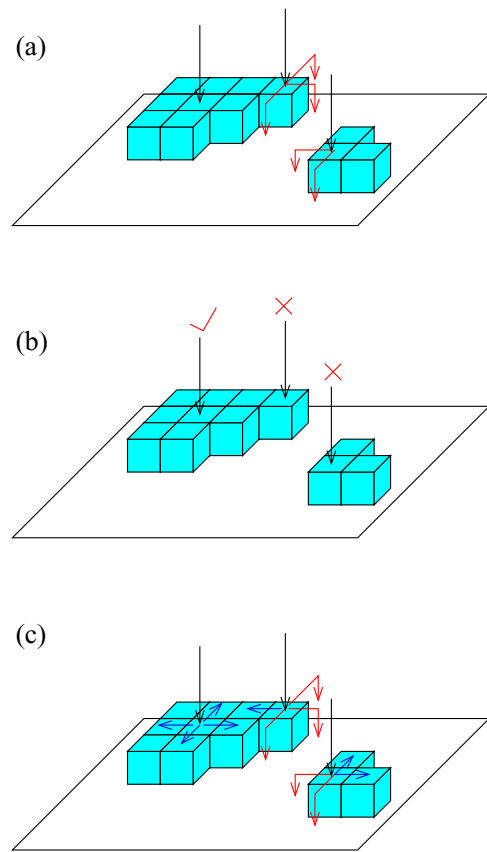

FIG. 1. Illustration of the rules of the deposition models, with black vertical arrows indicating the incidence point: (a) Family: red arrows indicate possible steps to lower columns; (b) RSOS: accepted and rejected aggregation attempts are shown; (c) LADP: possible first steps of the incident particle are indicated; red arrows show steps that lead to permanent aggregation, and blue arrows show steps to points in which diffusion may continue (up to a maximum of G steps).

surface diffusion) or when it has already executed G steps. This model was introduced in Ref. [32] to represent surface diffusion of adsorbed atoms or molecules in low-temperature film deposition. The possible first steps (immediately after incidence) of some particles in the LADP model are illustrated in Fig. 1(c).

Despite the relatively simple features of the LADP model, it can reproduce surface features of a model with collective surface diffusion of adatoms, namely, the CV model in conditions of irreversible adatom aggregation to lateral NN. The ratio R between diffusion coefficient and particle flux of this restricted CV model is related to G as [32]

$$R \sim 8G^{1.67}. \qquad (1)$$

Thus, the increase of temperature, which leads to the increase of the adatom diffusion coefficient, corresponds to an increase in the value of the parameter G.

Now we recall the hydrodynamic theories that represent the coarse-grained features of these deposition models.

The height fluctuations of the RSOS model are described by the KPZ equation [23]

$$\frac{\partial h}{\partial t} = \nu_2 \nabla^2 h + \lambda_2 (\nabla h)^2 + \eta(\vec{x}, t), \qquad (2)$$

where $h(\vec{r},t)$ is a height variable, $\nu_2 > 0$, $\lambda_2 \neq 0$, and η is a Gaussian white noise. The parameter ν_2 represents a surface tension. The nonlinear term appears when local growth occurs in the direction normal to the inclined interface and λ_2 is proportional to the velocity in that direction, as discussed in Ref. [22]. In the case of the RSOS model, restrictions to growth in inclined regions imply $\lambda_2 < 0$. KPZ scaling is observed in many electrodeposited films [33,34] and there are also observations in films deposited by vapor techniques [35].

The Family model is described in the hydrodynamic limit by the EW equation [25], which is Eq. (2) with $\lambda_2 = 0$.

The roughening in the LADP model is described by the Villain-Lai-Das Sarma (VLDS) [26,27] equation,

$$\frac{\partial h(\vec{r},t)}{\partial t} = -\nu_4 \nabla^4 h + \lambda_4 \nabla^2 (\nabla h)^2 + \eta(\vec{r},t), \qquad (3)$$

where $\nu_4 < 0$ and $\lambda_4 \neq 0$ are constants. The VLDS equation was proposed to represent roughening dominated by surface diffusion of the adsorbed species, which is expected in molecular beam epitaxy. In the case of $\lambda_4 = 0$, we obtain the Mullins-Herring equation [36].

Note that, in Eqs. (2) and (3), the constant external flux (expected in the deposition of a film) was omitted.

The average film height at time t is $\langle h \rangle \approx vt$, where v is the growth velocity: $v = 1$ for Family and LADP models; $v \approx 0.3217$ for the RSOS model [37]. As a film grows, the height fluctuations propagate in the directions parallel to the substrate and have increasing amplitude, as characterized by the time scaling of the surface roughness and of the autocorrelation function.

The surface roughness is the root-mean square height fluctuation, $W(t) \equiv \overline{\langle (h - \overline{h})^2 \rangle}^{1/2}$, where the overbars denote spatial average and the angular brackets denote configurational average. The roughness scales as $W \sim t^\beta$, with $\beta < 1$ for all models studied here. For KPZ, $\beta \approx 0.24$ [38,39]; for the other classes, smaller values of β are obtained [22]. This means that the amplitude of height fluctuations is much smaller than the average height at time t.

The autocorrelation function is defined as $\Gamma(s,t) \equiv \langle [\tilde{h}(\vec{r}_0 + \vec{s}, t) \tilde{h}(\vec{r}_0, t)]^2 \rangle$, where $s \equiv |\vec{s}|$ with $\vec{s}$ in x and y directions, $\tilde{h} \equiv h - \overline{h}$, and $\vec{r}_0$ spans the substrate columns. The characteristic length of decay of $\Gamma(s,t)$ is the correlation length ξ, which increases in time as a power law:

$$\xi \sim t^\nu. \qquad (4)$$

Here ν is the inverse of the dynamical exponent of the growth process (we do not use z to denote that exponent for avoiding confusion with the position z, which frequently appears in the text). In the EW class, $\nu = 0.5$ in any spatial dimension, which is expected for a diffusive correlation. In the KPZ class, lateral correlations lead to faster propagation; in two-dimensional substrates, $\nu \approx 0.620$ [38,39]. In diffusion-dominated roughening, correlations propagate slowly; in the VLDS class, $\nu \approx 0.30$ [27,40,41].

Simulations of all deposition models were performed on lattices with lateral size $L = 1024$. The number of deposited monolayers varied between 5×10^3 and 10^4. The LADP model was simulated with $G = 20$ and $G = 50$. Computer memory allocation restricts these maximal times, particularly
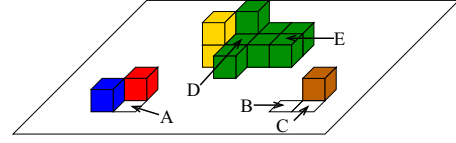

FIG. 2. Application of the rules for selecting the grain label at five aggregation positions. Colors indicate the labels of previously aggregated particles. The new particle label is (A) red or blue with equal probability; (B) new label; (C) brown; (D) green with probability 2/3 and yellow with probability 1/3; and (E) green.

because we store data for calculating the radius of gyration of each grain at each level z. The number of configurations produced with each deposition model varied between 5×10^2 and 10^3; different deposits were produced for the simulations of each model of grain nucleation and coarsening (Secs. III A and IV A), which improves the statistics.

III. GRAIN COARSENING WITH NUCLEATION AT THE SUBSTRATE

A. Model of nucleation and coarsening

A grain label is assigned to each deposited particle immediately after it reaches the final aggregation position. This position is determined by one of the deposition models of Sec. II and do not depend on grain labels. The grain boundary evolution is restricted to the outer surface of the film.

First, consider that the particle aggregates at $z = 1$, i.e., on the substrate. If this particle has no lateral neighbor, then a new label is assigned to it, different from the labels of all previously deposited particles. This means that it has a crystalline orientation different from the closest (but not neighboring) grains. On the other hand, if the particle aggregates at $z = 1$ and has one or more lateral neighbors, then one of these neighbors is randomly chosen and the particle receives its label. This represents island growth at the substrate by the incorporation of mobile atoms or molecules.

Now consider the case of a particle aggregated at $z > 1$. One of the NN-occupied sites (i.e., NN sites with previously aggregated particles) is randomly chosen and the new particle receives its label. The set of NN includes the neighbor below and the lateral neighbors. This model rule represents the competition of neighboring grains for the incorporation of new atoms or molecules.

These processes are illustrated in Fig. 2.

For comparison with the Saito-Omura model [15] and a related model in $2 + 1$ dimensions [16], note that they considered two different rules for grain label assignment.

In their first rule, if a particle aggregates at $z > 1$ and has a neighbor below, then the label of that neighbor is assigned to the particle, independently of the lateral neighbors. However, in the solid-on-solid deposition models studied here, a particle always has an occupied neighbor below it, thus the grain label of a column propagates only vertically, not laterally, i.e., there is no coarsening.

The second rule of grain assignment in Ref. [15] is the same as the one proposed here. For ballistic deposition, it showed deviations in the expected scaling of grain density. However, we believe that such rule is a more reasonable assumption
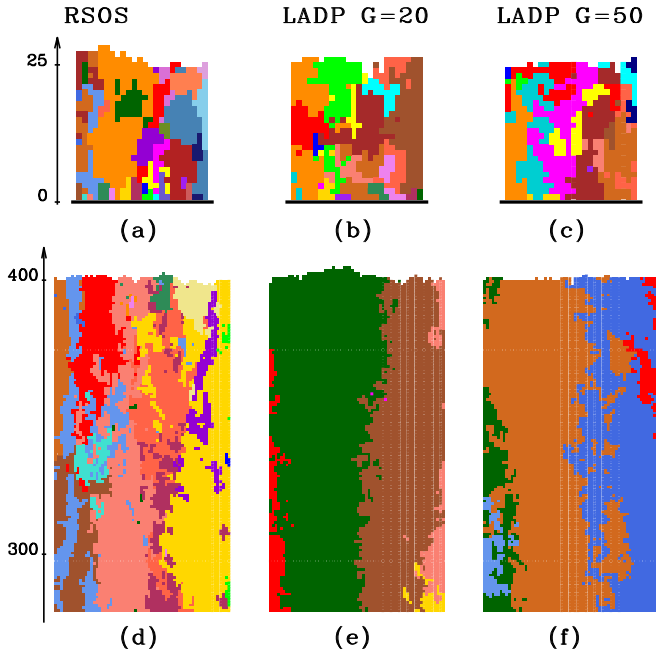
FIG. 3. (a)–(c) Cross sections of lateral size 32 of initial deposits; (d)–(f) cross sections of lateral size 64 of the upper layers of deposits with height ≈400, for the indicated deposition models and with grain nucleation only at the substrate.

FIG. 4. Top views with lateral size 64 of deposits with ≈400 layers for the indicated models and with grain nucleation only at the substrate.

for the grain competition because it allows coarsening in the absence of film voids.

B. Grain morphology

Figures 3(a)–3(c) show cross sections of initial deposits formed with the RSOS, the LADP $G = 20$, and the LADP $G = 50$ models, respectively. The sections were extracted from the films grown in much larger substrates ($L = 1024$).

Grains with very small sizes are formed on the substrate ($z = 1$) in RSOS deposition; the same feature is observed in deposition with the Family model. In deposition with the LADP model, the surface diffusion facilitates aggregation of mobile particles to the existing islands at $z = 1$, thus larger grains are formed, with size increasing with G; this is qualitatively observed in Figs. 3(b) and 3(c).

Figures 3(d)–3(f) show cross sections of the top part of deposits after deposition of ≈400 monolayers; again, they were extracted from the films grown in $L = 1024$.

The number of grains in the RSOS deposit is still large; the split of some grains in Fig. 3(d) shows that they may have significant branching. In the LADP deposits, grains are more compact and apparently larger. The sections in Figs. 3(e) and 3(f) also illustrate the coarsening process: as z increases, some grains increase their lateral sizes [e.g., the green one in Fig. 3(e) and the light brown one in Fig. 3(f)] while the lateral sizes of neighboring grains decrease.

Figure 4 shows 64×64 images of grain configurations at the surfaces of the films after deposition of ≈400 monolayers. The images for the RSOS and Family models confirm the large density of surviving grains and the branching of many of them (e.g., the red one in the RSOS and the dark violet one in the
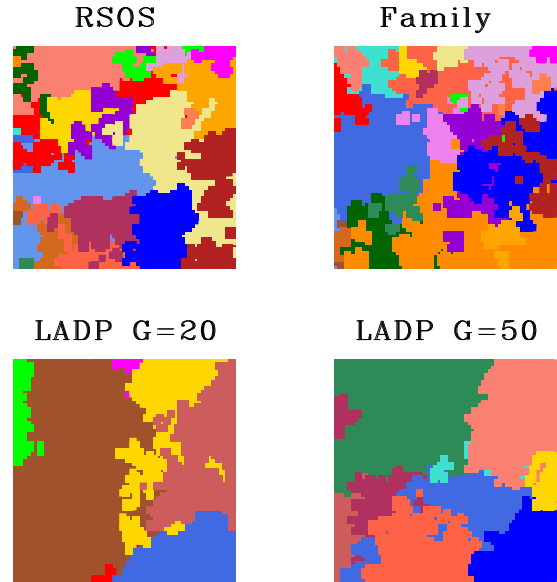
Family model). Grains formed with the LADP model are larger but may also have an irregular shape.

C. Scaling of grain density

Height fluctuations are correlated in a length ξ [Eq. (4)] and these flucutations are responsible for the lateral spread of the grain labels. The surviving grains at a given film height are those which could propagate laterally and cover the neighboring grains. Thus, their average lateral size l is expected to be of the same order of magnitude of ξ. This argument rephrases that of Saito and Omura for grain coarsening in the BD model [15].

Although the grains have irregular shapes, rough borders, and may form branches, the top images of Fig. 4 do not suggest fractal morphology. For instance, their shapes contrast with the highly branched fractal structure of diffusion-limited aggregates [42] or of the initial islands of the deposition-diffusion-aggregation model with critical island size $i = 1$ [5,43]. Thus, the average lateral area (parallel to the xy plane) of the grains is expected to scale as that of compact two-dimensional structures, which is of order $l^2 \sim \xi^2 \sim t^{2\nu}$. The density ρ_0 of surviving grains, defined as the number of grains per surface site, scales as

$$\rho_0 \sim t^{-\gamma}, \quad \gamma = 2\nu. \tag{5}$$

The estimates of γ for the deposition models studied here are ≈1.24 for RSOS; 1 (exact) for Family; and ≈0.60 for LADP.

Let $M_0(t)$ be the average number of particles of surviving grains at time t (particles at the film surface of below this surface). The scaling M_0 can be obtained from the scaling of l^2 as

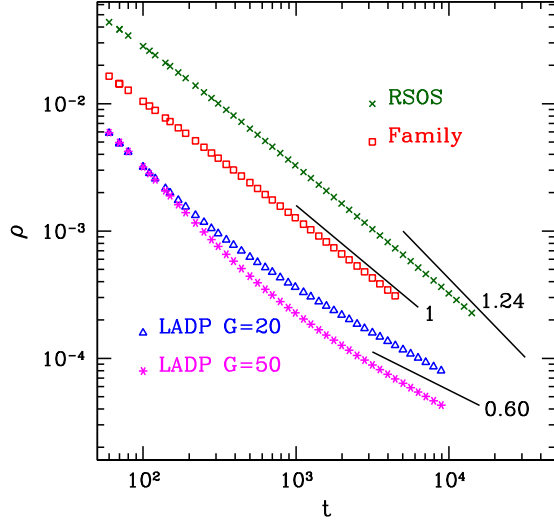$$M_0 \sim \int_0^t l^2 \, dt \sim t^{\gamma+1}. \tag{6}$$

FIG. 5. Density of surface grains as a function of time in the model of grain nucleation only at the substrate and deposition with Family (red squares), RSOS (green crosses), LADP $G = 20$ (blue triangles), and LADP $G = 50$ (magenta stars) models. The solid lines have the slopes predicted for each growth class.

FIG. 6. Square radius of gyration as a function of the height z in the model of grain nucleation only at the substrate: (a) Family (red squares) and RSOS (green crosses) deposition; dashed lines are linear fits, with slopes 1.03 and 1.10, respectively (expected values: 1 and 1.24); (b) LADP deposition with $G = 20$ (blue triangles) and $G = 50$ (magenta stars); dashed lines are linear fits for $z \geqslant 10^3$, with slopes 0.68 and 0.73, respectively (expected value 0.60).

Figure 5 shows the time evolution of the grain density in four deposition models. The expected slopes (values of γ) are indicated for comparison with the trends of the data at the longest simulated times.

Films grown with the Family model have a grain density very close to the expected decay for thicknesses ~ 500 layers and more. Films grown with the RSOS model show similar scaling until thicknesses ~ 5000 layers (corresponding to $t \approx 1.5 \times 10^4$), which means that the KPZ nonlinearity has little effect on the grain density. This result is surprising because RSOS is well known as a model with small corrections in the KPZ roughness; on the other hand, we recall that deviations from the asymptotic scaling were also observed in grain coarsening in ballistic deposition with the present rule for label assignment [15].

The grain density in the LADP films have clear crossovers for thicknesses between ~ 500 and ~ 1000 layers. For smaller thicknesses, the slopes of the plots in Fig. 5 suggest $\gamma > 1$, which is much larger than the asymptotic value ≈ 0.60. The films grown with $G = 20$ show slope close to that value for the largest thicknesses ($\sim 10^4$ layers), but the slope for $G = 50$ is still near 0.70. Despite these deviations, the temperature effect is clear after deposition of approximately 500 layers: the grain density decreases as G increases, which means that the higher the temperature the larger the grains.

D. Scaling of grain shape

Here we characterize the grain shape for each position z above the substrate, i.e., in each horizontal slice of the film, by an average square radius of gyration $\langle R_2(z) \rangle$. For each grain, the radius of gyration at a given height z is defined as $R_2 = \overline{(x - \overline{x})^2 + (y - \overline{y})^2}$, with the average taken over all particles of the grain at that height. Then $\langle R_2(z) \rangle$ is obtained by averaging over all grains at that height (the film slice).
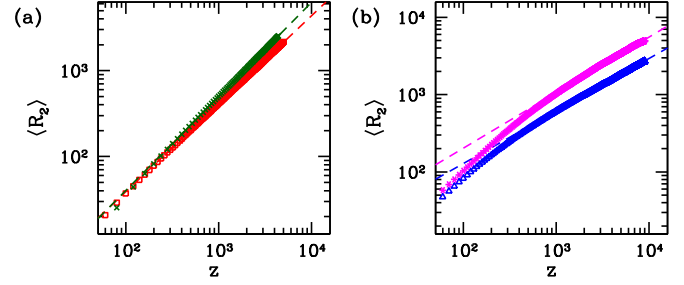
The height fluctuations among the surviving grains or in a single grain surface are expected to be of the same order of (or smaller than) the surface roughness W of the whole film surface, which in turn is much smaller than the average film height $\langle h \rangle \approx vt$, as discussed in Sec. II. Thus, although each point of the grain attains a given height z at a slightly different time (due to those fluctuations), $\langle R_2(z) \rangle$ is representative of the surviving grains at a coarse-grained time $t \approx z/v$.

We expect that $\langle R_2(z) \rangle$ scales as the average area of exposed grains, i.e., as the inverse of the grain density, while z increases linearly in time. Using Eq. (5), we obtain

$$\langle R_2 \rangle \sim z^\gamma. \tag{7}$$

In Fig. 6(a) we show $\langle R_2 \rangle$ as a function of z for the RSOS and Family models, and in Fig. 6(b) we show the same quantities for the LADP models with $G = 20$ and $G = 50$.

For the Family model, the slope of the plot is actually very close to the expected γ. For the RSOS model, a deviation of $\approx 10\%$ is again observed, with an apparently weak effect of the nonlinearity up to $z \approx 5 \times 10^3$. In the LADP model with $G = 20$ or $G = 50$, the typical radii of gyration are larger than those of the other growth models up to $t \sim 10^4$. The slopes are near 0.7 in the thickness range $10^3 \leqslant z \leqslant 9 \times 10^3$, differing from the expected γ by $\approx 17\%$. However, they are much smaller than the slopes of the models with relaxation dominated by surface tension. This suggests that the average grain shape may be a suitable quantity for distinguishing the kinetics dominated by surface diffusion, possibly complementary to the study of surface roughening. Also note that the average radius of gyration increases as G increases in Fig. 6(b), corresponding to a temperature increase.

E. Comparison with other models

The polycrystalline structures illustrated in Figs. 3 and 4 for the LADP model resemble those presented in some previous works on film growth models in which nucleation is possible only at the substrate.

Reference [7] analyzed the island growth in the sub-monolayer regime and shows monolayer films with shapes similar to those of Fig. 4. Reference [6] proposed a model for polycrystalline Al film growth which included grain

boundary diffusion and also showed grain coarsening. A similar approach was considered in Ref. [8], and effects of temperature and adhesion to the substrate were studied. The models for pulsed-laser deposition in Ref. [12] and of electrodeposition in Ref. [11] also show grain shapes similar to those of Figs. 3 and 4. Those works show increase of grain size with the temperature, but scaling relations for characteristic sizes as a function of temperature or time were not analyzed.

The grain shapes obtained in some two-dimensional models [9,10,13] are also similar to those of the cross sections of Fig. 3.

IV. GRAIN COARSENING WITH NUCLEATION AT ALL LAYERS

A. Model of nucleation and coarsening

In this model, the aggregation of a new particle at a final position is also determined by one of the models of Sec. II. The grain label is also assigned to the particle immediately after its aggregation, thus restricting the grain boundary evolution to the outer surface of the deposit.

When the new particle aggregates, a new label is assigned to it with probability p, independently of its neighborhood. This label is different from all previous labels, in order to represent a crystalline orientation different from all the closest grains (which may eventually compete for growth). Otherwise, with probability $1 - p$, the same rules of Sec. III A for label assignment are applied to the new aggregated particle.

The model of Sec. III A is consequently the case $p = 0$. Here we always consider $p \ll 1$, thus the probability that the aggregated particle has a label different from its neighbors is very small. Despite this condition, the continuous creation of new grains leads to remarkable changes in the coarsening process at long times.

Our simulations for all deposition models were performed for $10^{-5} \leqslant p \leqslant 10^{-3}$. The number of deposited layers varied between 5×10^3 and 5×10^4, depending on the model and on the value of p.

B. Grain morphology

Figures 7(a)–7(c) shows cross sections of films deposited with the same models of Figs. 3(d)–3(f), but now with nucleation at all heights. The presence of elongated large grains is also observed. However, many small grains appear as spots in the middle of the large grains; this is particularly clear when the sections of the LADP model are compared.

The same features are observed in the images of grain configurations at the film surfaces, shown in Figs. 7(d)–7(f). There are large grains with rough boundaries and possible branching, similarly to those of Fig. 4. However, the number of small grains is clearly larger as a consequence of recent nucleations. The images have lateral size 64 and the probability of new nucleation is $p = 10^{-3}$, thus approximately four new grains are expected to nucleate for each deposited layer.

C. Crossover scaling

Figure 8 shows the evolution of the surface grain density for four deposition models and three values of p. At short times, ρ decays as a power law, similarly to the case with
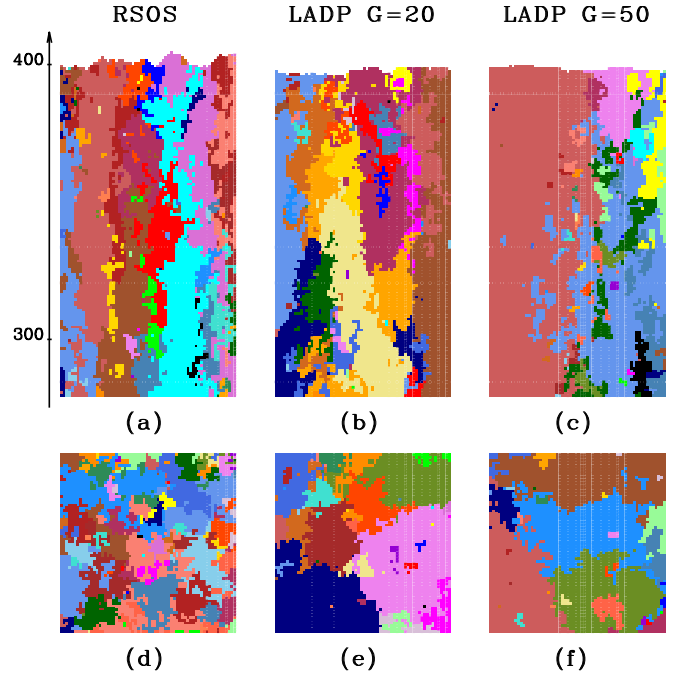

FIG. 7. (a)–(c) Cross sections of lateral size 64 of the upper layers of deposits with height ≈ 400; (d)–(f) show top views of the same size, for the indicated deposition models and grain nucleation at all heights with $p = 10^{-3}$.

nucleation only at the substrate. At long times, it saturates due to the creation of new grains while other grains are buried as a consequence of coarsening.

The crossover between these two regimes is expected when the rate of creation of new grains, r_P, matches the rate of annihilation of the existing grains, r_A. These rates
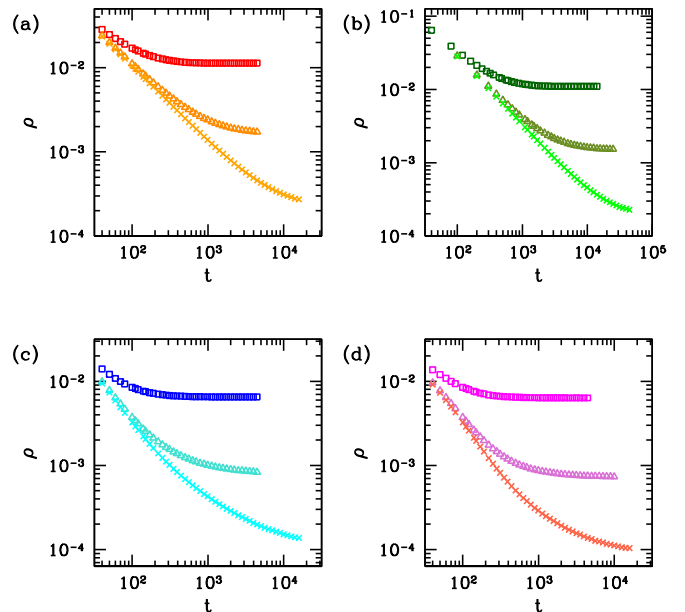

FIG. 8. Density of surface grains as a function of time for grain nucleation at all heights, with $p = 10^{-3}$ (squares), $p = 10^{-4}$ (triangles), and $p = 10^{-5}$ (crosses) and the deposition models: (a) Family; (b) RSOS; (c) LADP with $G = 20$; and (d) LADP with $G = 50$.

are measured in number of grains per substrate column per unit time. Since one layer is deposited in a time $\tau = 1/v$, we have $r_P = p/\tau = pv$. From Eq. (5), the annihilation rate is $r_A = d\rho_0/dt \sim t^{-\gamma-1}$. Considering that $v \sim 1$ for all models, the crossover time estimated when $r_P \sim r_A$ is

$$t_c \sim p^{-1/(\gamma+1)} = p^{-1/(2\nu+1)}. \qquad (8)$$

The scaling relation for r_A may include a model-dependent amplitude, but this amplitude is difficult to estimate due to the slow convergence to the scaling of Eq. (5). For this reason, no such amplitude was considered in the above derivation.

Equation (8) gives decays as $p^{-0.5}$ for Family, $p^{-0.45}$ for RSOS, and $p^{-0.63}$ for LADP models. In Fig. 8, t_c may be estimated as a point in which a deviation from the initial power-law begins; this confirms that t_c increases as p decreases (with the same deposition model).

The saturation grain density is of the order of the density at $t = t_c$:

$$\rho_c \sim t_c^{-\gamma} \sim p^{\gamma/(\gamma+1)} = p^{\nu/(\nu+1/2)}. \qquad (9)$$

This result gives decays as $p^{0.5}$ for Family, $p^{0.55}$ for RSOS, and $p^{0.38}$ for LADP models. The results in Fig. 8 are also qualitatively consistent with the decrease of ρ_c as p decreases.

Inspection of Figs. 8(c) and 8(d) also shows that the surface grain density saturates at smaller values for larger G in LADP models (the difference looks small in the logarithmic scale of those plots). This is again consistent with the increase of grain size with the temperature.

Estimates of rho_c for each model and each p can be obtained at the longest simulated times. The crossover time t_c can be quantitatively estimated as the time in which the density ρ is 1% larger than ρ_c. Plots of t_c as a function of p (not shown here) are consistent with the power law scaling predicted in Eq. (8), but the exponents for $p \leqslant 10^{-4}$ differ $\approx 10\%$ from the predicted values for all models. The plots of rho_c as a function of p are also consistent with a power law, as predicted in Eq. (9), but in this case the exponents are very different from the estimates presented above. We believe this is a consequence of the small values of t_c analyzed here (in the range $[10^2, 10^4]$) because the model with nucleation only at the substrate (Sec. III C) has already shown huge corrections in the density scaling, as illustrated, i.e., in Fig. 5. Thus, it is expected that such corrections also affect the crossover scaling of the present model.

At t_c, the average grain mass is given by Eq. (6), even considering that a large number of small grains (of order pt_c) have been added to the deposit; this crossover mass is

$$M_c \sim t_c^{\gamma+1} \sim p^{-1}. \qquad (10)$$

A crossover scaling in the form $\rho = \rho_0 f(t/t_c)$ may be proposed for the surface grain density, but this relation is also affected by large scaling corrections, as discussed above. Figure 5 shows that the asymptotic scaling of the models with nucleation only at the substrate is reached only at $t \sim 10^4$ or longer. Thus, we expect that the quantitative predictions of the crossover scaling can be observed only if t_c is of this order or larger. However, the corresponding thicknesses will be much larger than the ones suitable to model real thin films ($\lesssim 10\,\mu m$).
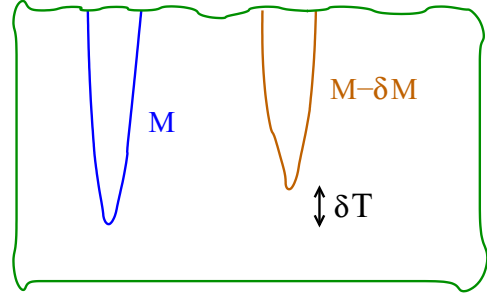

FIG. 9. Scheme of a film section with two grains formed in a time difference δt.

D. Mass and size distributions

The model with grain nucleation at all heights has the same basic mechanisms of other models that combine cluster agglomeration (coarsening) and particle injection. Takayasu and coworkers [28,44] introduced this type of model considering diffusion of clusters in a one-dimensional lattice with continuous particle flux. When mass is conserved, the clusters increase in size and their density decreases as a power law; with particle injection, the density fluctuates around an average value at long times.

An interesting feature of Takayasu models is the power law decay of the cluster size distribution in the case of particle injection, with an exponent related to the coarsening exponent of the mass-conserved system [28,44]. Swift *et al.* [29] proposed a scaling approach to connect a variety of related coarsening processes with and without mass conservation in any spatial dimension. Here we extend their approach to our model and obtain the scaling of distributions of grain mass, height, and radius of gyration.

Let $P(M,t,p)$ be the probability that a grain has mass M at time t in the model with new grain formation rate p. Considering the coarsening at long times, i.e., $t \gg t_c$, we expect that the system reaches a time-independent grain size distribution. Thus we focus on $P(M,p)$, which is the probability that a grain has mass M after the saturation of grain density.

The leading term of the distribution $P(M,p)$ is assumed to have the decay $M^{-\tau}$, with the exponent τ to be determined. This form is valid for large grains, i.e., it excludes grains with $M \sim 1$. A cutoff of the power law is expected for $M \gg M_c$ because very large masses are highly improbable when new grains are formed. A scaling assumption is thus proposed as

$$P(M,p) = M^{-\tau} F\left(\frac{M}{M_c}\right) = M^{-\tau} F(Mp), \qquad (11)$$

where F is a scaling function and Eq. (10) was used. For $u \lesssim 1$, $F(u)$ is approximately constant and the power law is expected (note that $u \gg p^{-1}$ is required to exclude the grains with $M \sim 1$). The cutoff is expected at some $u \gg 1$, after which $F(u)$ becomes a rapidly decreasing function of its variable.

In order to calculate the exponent τ, we consider the scheme of Fig. 9 with two grains at the same height, with masses M and $M - \delta M$ and ages T and $T - \delta T$, respectively. The age T is the time interval since the nucleation of the grain. Both masses are of an order of magnitude near that of M_c. The mass of these large surviving grains obeys Eq. (6) with t replaced by the age T. This can be used to relate the difference of mass

between those grains and the time interval of their nucleation:

$$M \sim T^{\gamma+1} \Rightarrow \delta M \sim T^{\gamma} \delta T. \qquad (12)$$

The probability of finding grains with mass in the interval $[M - \delta M, M]$ is $P(M,p)\delta M$. It is proportional to the total number of grains that reached the same height as the two grains in Fig. 9 and that were nucleated in the time interval ΔT, i.e., the total number of exposed grains with ages intermediate between the ages of those two grains. This number is proportional to $p\delta T$, which is the total number of grains nucleated in the time interval ΔT. Thus

$$P(M,p)\delta M \sim p\delta T \Rightarrow P(M,p) \sim pT^{-\gamma}, \qquad (13)$$

where Eq. (12) was used. Using this result, Eqs. (8) and (10) with t replaced by the age T, we obtain the probability density for a mass of order M_c as

$$P(M_c,p) \sim M_c^{-1} M_c^{-\gamma/(\gamma+1)}. \qquad (14)$$

Consequently, the exponent in Eq. (11) is

$$\tau = \frac{2\gamma+1}{\gamma+1} = \frac{4\nu+1}{2\nu+1}. \qquad (15)$$

This gives $\tau = 1.5$ for Family, $\tau \approx 1.55$ for RSOS, and $\tau \approx 1.38$ for LADP models.

An alternative form of the scaled mass distribution is

$$P(M,p) = p^{\tau} G(Mp). \qquad (16)$$

In this case, the scaling function G has a power-law decay with M, with exponent τ. Such decay may fail for $M \sim 1$ ($Mp \lesssim p$) and crosses over to a faster decay for some M much larger than M_c ($Mp \gg 1$).

Figure 10 shows $p^{-\tau}P(M,p)$ as a function of Mp for the four growth models and several values of p, considering the exponents τ given in Eq. (15). The good data collapse of each plot confirms the scaling ansatz. The power law decay of the mass distribution is clear in more than five decades of M and more than seven decades of P for all models. Also note that this decay is always observed for $pM \sim 1$, i.e., $M \sim M_c$; this is consistent with the arguments used to justify Eqs. (11) and (15). The deviations from the power law to faster decays occur for $M/M_c \sim 10^3$ or larger, which is also consistent with that reasoning.

The slopes of the plots of the Family and of the RSOS models [Figs. 10(a) and 10(b)], obtained from linear fits, differ less than 3% from the predicted values of τ. Linear fits of the plots of the LADP model [Figs. 10(c) and 10(d)] have slopes near 1.45, which is 5% larger than the theoretical prediction shown in those plots.

Analogous scaling arguments show that the distributions of aggregate height h and of square radius of gyration R_2 also have power law decays:

$$P(h,p) = h^{-\Delta} F_1\left[\frac{h}{h_c(p)}\right], \quad \Delta = \gamma+1, \qquad (17)$$

where F_1 is a scaling function and

$$h_c \sim t_c \sim p^{-1/(\gamma+1)}, \qquad (18)$$

$$P(R_2,p) = R_2^{-\sigma} F_2\left[\frac{R_2}{R_{2c}(p)}\right], \quad \sigma = 2, \qquad (19)$$
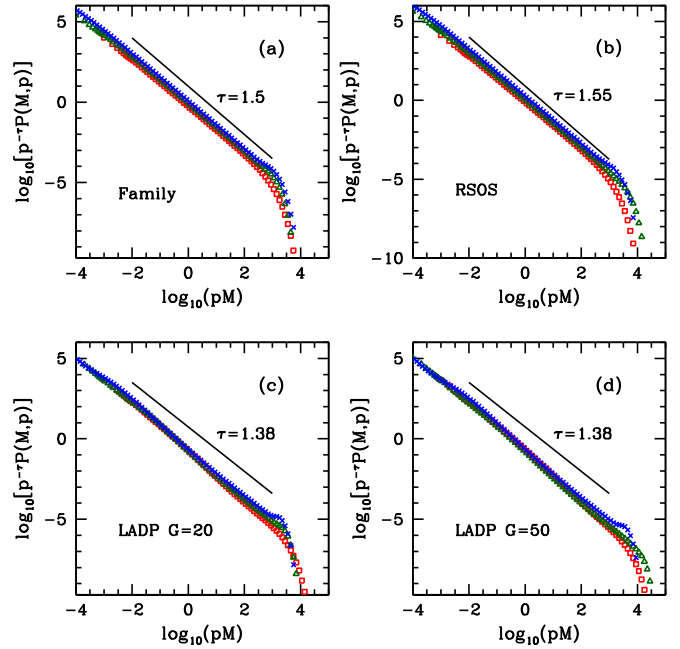

FIG. 10. Scaled distributions of grain mass for grain nucleation at all heights, with $p = 10^{-3}$ (red squares), $p = 10^{-4}$ (green triangles), and $p = 10^{-5}$ (blue crosses), and the deposition models indicated in the plots. The solid lines have the theoretically predicted slopes for the power law decays. For LADP models with $p = 10^{-5}$, the bumps of the plots at $pM \sim 10^3$ are consequences of the limited simulation time, which interrupted the growth of the largest grains.

where F_2 is a scaling function and

$$R_{2c} \sim p^{-\gamma/(\gamma+1)}. \qquad (20)$$

Note that the exponents of the above power-law distributions are not very different among the different classes of deposition models. Indeed, if the distributions of Figs. 10(a)–10(d) (for different classes) were shown in the same plot, the slopes would be approximately the same (≈ 1.5). For the grain height distribution, all slopes are near 0.5, and the exponent σ of the distribution of R_2 is the same for all models. Our numerical results are also consistent with these values.

E. Grain shape

For $t \gg t_c$, we measured the square radius of gyration R_2 of each grain at each height h measured from the bottom layer of the grain (i.e., $h = 0$ at the layer in which the grain is nucleated). Averaging over all grains at $t > t_c$, we obtain the average radius of gyration $\langle R_2 \rangle$ as a function of the height h, which characterizes the typical shape of the grains.

These quantities have definitions similar to $\langle R_2 \rangle$ and z of the model with nucleation limited to the substrate. However, in the present model, $\langle R_2 \rangle$ and h have effective upper bounds that depend on p, since finding very large grains ($M/M_c > 10^3$) is highly improbable; see Figs. 10(c) and 10(d).

The typical heights and typical radii of gyration of the grains are of the order of h_c and R_{2c}, respectively, which are related as $R_{2c} \sim h_c^{\gamma}$. Thus, we expect

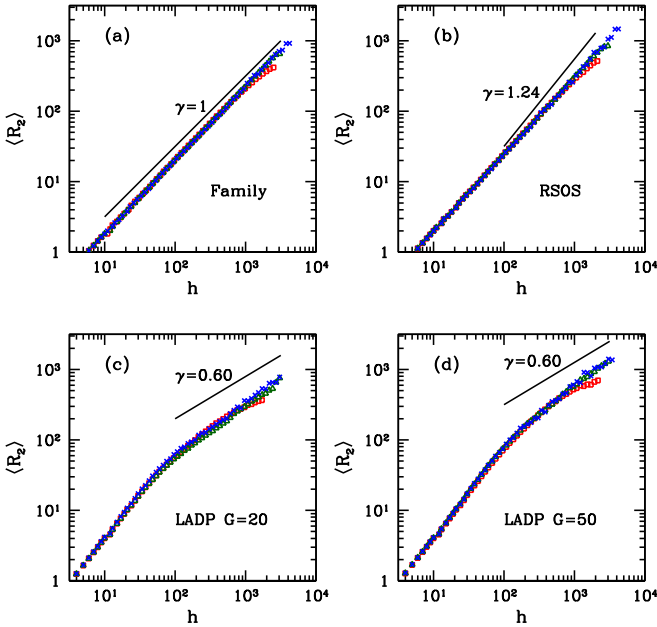$$\langle R_2 \rangle \sim h^{\gamma}. \qquad (21)$$

FIG. 11. Square radius of gyration as a function of grain height for the model with nucleation at all heights, with the same symbols of Fig. 10. The solid lines have the theoretically predicted slopes.

In Fig. 11 we show $\langle R_2 \rangle$ as a function of h for four deposition models and three values of p. For $h \sim 100$ or larger, power law scaling is observed in all cases. The values of exponents are clearly different when results for roughening controlled by surface tension (Family, RSOS) and controlled by surface diffusion (LADP) are compared: the plots of the former give exponents 1.04 (Family) and 1.10 (RSOS), and the plots of the latter give exponents 0.70 (LADP $G = 20$) and 0.77 (LADP $G = 50$); the theoretical predictions are shown in the corresponding plots. Thus, in this model, the average grain shape is also a suitable quantity for distinguishing surface tension or surface diffusion as the dominant mechanism of roughening.

In Ref. [14], a two-dimensional model of polycrystalline film growth was studied considering the possibility of nucleation at all heights and effects of grain switching and vacancies. It was shown that the grain structure reached a steady state, which corresponds to the crossover to a saturation in the surface density discussed here. An increase in the grain aspect ratio with the grain diameter was also shown in that work. This is consistent with the results obtained here, meaning that the average diameter increases slower than the average height of the grains; indeed, Eq. (21) shows that the diameter increases as $\sim h^{\nu}$ and $\nu < 1$ for any film growth dynamics.

V. POSSIBLE APPLICATIONS

The comparison of our results with available experimental data on polycrystalline films may be a first step for the application of our model or for its improvement to describe grain sizes and shapes quantitatively.

A particularly interesting application is the electrodeposition of Cu_2O in different substrates (Si and a Ni layer on Si), in which some grains formed at the substrates grow up

to heights $\sim 1 \mu$m with time increasing diameter [45]. The position of the minimum of the auto-correlation function is in good agreement with the typical grain size observed in AFM images and scales with an exponent ν near that of the MH equation. The presence of MH roughening in various length scales was confirmed by comparison of distributions of heights, roughness, and extremal heights. Thus, the main control of the grain coarsening is the surface roughening, as proposed in our model.

Using electron backscatter diffraction, recent works analyzed the orientations of grains of electrodeposited Zn films on steel [46,47]. Some images suggest coarsening of grains similar to our model of nucleation only at the substrate, with some grains increasing in lateral size and burying neighboring grains. The focus of those works was the grain misorientation relatively to the substrate and the nucleation process, but an investigation of grain sizes and shapes would certainly be interesting for comparison with available models.

In the pulsed-laser deposition (PLD) of ZnO films of Ref. [48], the grain size was shown to increase linearly in time, which corresponds to $\nu = 1$ in our model and gives $\gamma \approx 2$. These exponents indicate that the lateral propagation of fluctuations is much faster than in the deposition models studied here. This may be useful for the development of PLD models.

VI. CONCLUSION

We proposed a lattice model to represent coarsening of crystalline grains during thin film deposition. The incorporation of new atoms or molecules is determined by deposition models in different universality classes, with no effect of the grain structure. The grain boundary evolution at the film surface is then determined by a probabilistic competition of neighboring grains. These assumptions allow an initial investigation of the effects of kinetic roughening on grain structure.

First we extended a previous model that considered nucleation of grains only at the substrate. Simulations show a decay of the grain density with the film thickness in reasonable agreement with a scaling approach that relates the typical lateral size of a grain and the correlation length of the deposition kinetics (involving the dynamical exponent). The scaling of the average radius of gyration with the film thickness has the same exponent of that relation. Simulations in thicknesses above ~ 500 monolayers show significant difference between the exponent estimates for growth dominated by surface tension and growth dominated by surface diffusion.

Subsequently, we extended that model by considering nucleation of new grains during the deposition, with grain labels representing orientations different from all previous grains. The surface grain density crosses over from the initial power law decay to a saturation regime; the time, grain mass, and surface grain density at the crossover are estimated as a function of the rate of nucleation of new grains. The long time distributions of grain mass, height and radius of gyration have power law decays which are explained by a scaling approach that predicts the exponents in terms of the dynamical exponent of kinetic roughening. These results are confirmed by simulations that span several orders of magnitude of those quantities and of their probability densities. The

characterization of the grain shape is done by measuring the radius of gyration at each height h relative to the base of the grain. Simulations show a scaling of the average radius with h, for $h \approx 100$ and larger, with exponents consistent with theoretical predictions and whose values are also clearly distinct for roughening dominated by surface tension and by surface diffusion.

In the deposition of real films, grain coarsening leads to the elimination of many small grains whose atoms or molecules migrate to larger grains; this implies surface and subsurface movement of grain boundaries. Instead, the present model considers immobile grain boundaries, so that small grains remain at the film even after they are covered and cannot grow. However, we believe that the dynamics of these small grains do not change the main results of this work. The morphological properties of large grains (average sizes, size distribution, etc.) are related to the long wavelength scaling of surface fluctuations via the dynamical exponent (or the related exponent γ). This exponent is universal for each growth class, i.e., it depends only on basic symmetries of the deposition process. Details of short scale fluctuations do not affect those

properties, and one of such details seems to be the presence or absence of very small grains.

On the other hand, our assumption that the surface growth dynamics is independent of local crystalline structure is not realistic in many cases. For instance, different adsorption rates at the surface of different grains may develop surface fluctuations with other relevant length scales. Different mechanisms of atom or molecule aggregation near the grain boundaries is another important ingredient that should be considered for an accurate description of real polycrystalline films. However, despite the limitations of the models presented here, they may be a reasonable approximation for some systems and their study is a first step to understand how the film growth kinetics affects the polycrystalline structure. This study may also motivate the search for nontrivial features such as the power law mass distribution and the radius-height scaling in experiments.

ACKNOWLEDGMENT

[1] C. V. Thompson, Annu. Rev. Mater. Sci. **30**, 159 (2000).

[2] D. J. Srolovitz, J. Vac. Sci. Technol. **4**, 2925 (1986).

[3] R. W. Smith, J. Appl. Phys. **81**, 1196 (1997).

[4] S. Clarke and D. D. Vvedensky, J. Appl. Phys. **63**, 2272 (1988).

[5] J. W. Evans, P. A. Thiel, and M. C. Bartelt, Surf. Sci. Rep. **61**, 1 (2006).

[6] H. Huang, G. H. Gilmer, and T. D. de la Rubia, J. Appl. Phys. **84**, 3636 (1998).

[7] P. Bruschi, A. Nannini, and F. Pieri, Phys. Rev. B **63**, 035406 (2000).

[8] J. E. Rubio, M. Jaraiz, I. Martin-Bragado, J. M. Hernandez-Mangas, J. Barbolla, and G. H. Gilmer, J. Appl. Phys. **94**, 163 (2003).

[9] J. Liu, C. Liu, and P. P. Conway, Electrochem. Comm. **11**, 2207 (2009).

[10] J. Liu, C. Liu, and P. P. Conway, Electrochim. Acta **97**, 132 (2013).

[11] T. Treeratanaphitak, M. D. Pritzker, and N. M. Abukhdeir, Electrochim. Acta **121**, 407 (2014).

[12] X. Tan, Y. C. Zhou, and X. J. Zheng, Surf. Sci. **588**, 175 (2005).

[13] Y. Y. Huang, Y. C. Zhou, and Y. Pan, Physica E **41**, 1673 (2009).

[14] S. Ruan and C. A. Schuh, J. Appl. Phys. **107**, 073512 (2010).

[15] Y. Saito and S. Omura, Phys. Rev. E **84**, 021601 (2011).

[16] K. Osada, H. Katsuno, T. Irisawa, and Y. Saito, J. Semicond. **37**, 092001 (2016).

[17] C. Deng and C. A. Schuh, Phys. Rev. Lett. **106**, 045503 (2011).

[18] P. R. Cantwell, M. Tang, S. J. Dillon, J. Luo, G. S. Rohrer, and M. P. Harmer, Acta Mater. **62**, 1 (2014).

[19] M.-C. Chen, C. Yang, and L. I, Phys. Rev. E **90**, 050401(R) (2014).

[20] A. R. Kalidindi, T. Chookajorn, and C. A. Schuh, JOM **67**, 2834 (2015).

[21] J. Krug, Adv. Phys. **46**, 139 (1997).

[22] A. L. Barabási and H. E. Stanley, *Fractal Concepts in Surface Growth* (Cambridge University Press, Cambridge, 1995).

[23] M. Kardar, G. Parisi, and Y.-C. Zhang, Phys. Rev. Lett. **56**, 889 (1986).

[24] D. J. Eaglesham, J. E. Bower, M. A. Marcus, M. Gross, and S. Merchant, Appl. Phys. Lett. **71**, 219 (1997).

[25] S. F. Edwards and D. R. Wilkinson, Proc. R. Soc. London **381**, 17 (1982).

[26] J. Villain, J. Phys. I France **1**, 19 (1991).

[27] Z.-W. Lai and S. Das Sarma, Phys. Rev. Lett. **66**, 2348 (1991).

[28] H. Takayasu, I. Nishikawa, and H. Tasaki, Phys. Rev. A **37**, 3110 (1988).

[29] M. R. Swift, F. Colaiori, A. Flammini, A. Maritan, A. Giacometti, and J. R. Banavar, Phys. Rev. Lett. **79**, 3278 (1997).

[30] F. Family, J. Phys. A: Math. Gen. **19**, L441 (1986).

[31] J. M. Kim and J. M. Kosterlitz, Phys. Rev. Lett. **62**, 2289 (1989).

[32] F. D. A. Aarão Reis, Phys. Rev. E **81**, 041605 (2010).

[33] M. Castro, R. Cuerno, A. Sánchez, and F. Domínguez-Adame, Phys. Rev. E **57**, R2491 (1998).

[34] R. Cuerno and M. Castro, Phys. Rev. Lett. **87**, 236103 (2001).

[35] R. A. L. Almeida, S. O. Ferreira, T. J. Oliveira, and F. D. A. Aarão Reis, Phys. Rev. B **89**, 045309 (2014).

[36] W. W. Mullins, J. Appl. Phys. **28**, 333 (1957); C. Herring, *ibid.* **21**, 301 (1950).

[37] T. J. Oliveira, S. G. Alves, and S. C. Ferreira, Phys. Rev. E **87**, 040102(R) (2013).

[38] J. Kelling and G. Ódor, Phys. Rev. E **84**, 061150 (2011).

[39] A. Pagnani and G. Parisi, Phys. Rev. E **92**, 010101(R) (2015).

[40] H. K. Janssen, Phys. Rev. Lett. **78**, 1082 (1997).

[41] F. D. A. Aarão Reis, Phys. Rev. E **70**, 031607 (2004).

[42] T. A. Witten, Jr. and L. M. Sander, Phys. Rev. Lett. **47**, 1400 (1981).

[43] P. Jensen, A.-L. Barabási, H. Larralde, S. Havlin, and H. E. Stanley, Phys. Rev. E **50**, 618 (1994).

[44] H. Takayasu, Phys. Rev. Lett. **63**, 2563 (1989).

[45] I. S. Brandt, V. C. Zoldan, V. Stenger, C. C. Plá Cid, A. A. Pasa, T. J. Oliveira, and F. D. A. Aarão Reis, J. Appl. Phys. **118**, 145303 (2015).

[46] T. Greul, C. Comenda, K. Preis, J. Gerdenitsch, R. Sagl, and A. W. Hassel, Electrochim. Acta **113**, 797 (2013).

[47] T. Greul, J. Gerdenitsch, C. Comenda, R. Sagl, M. Arndt, J. Duchoslav, and A. W. Hassel, Surf. Coat. Technol. **253**, 8 (2014).

[48] A. González-González, C. Polop, and E. Vasco, Phys. Rev. B **86**, 045434 (2012).